HU Binding to Bent DNA: A Fluorescence Resonance Energy Transfer and Anisotropy Study†

Kristi Wojtuszewski‡ and Ishita Mukerji*

Molecular Biology and Biochemistry Department, Molecular Biophysics Program, Wesleyan University, Middletown, Connecticut 06459-0175

Received July 3, 2002; Revised Manuscript Received January 15, 2003

ABSTRACT: HU, an architectural DNA-binding protein, either stabilizes DNA in a bent conformation or induces a bend upon binding to give other proteins access to the DNA. In this study, HU binding affinity for a bent DNA sequence relative to a linear sequence was investigated using fluorescence anisotropy measurements. A static bend was achieved by the introduction of two phased A_4T_4 tracts in a 20 bp duplex. Binding affinity for 20 bp duplexes containing two phased A-tracts in either a 5′-3′ or 3′-5′ orientation was found to be almost 10-fold higher than HU binding to a random sequence 20 bp duplex (6.1 vs 0.68 μM^{-1}). The fluorescence technique of resonance energy transfer was used to quantitatively determine the static bend of the DNA duplexes and the HU-induced bend. DNA molecules were 5′-end labeled with fluorescein as the donor or rhodamine as the acceptor. From the efficiency of energy transfer, the end-to-end distance of the DNA duplexes was calculated. The end-to-end distance relative to DNA contour length (R/R_C) yields a bend angle for the A-tract duplex of 45 ± 7° in the absence of HU and 70 ± 3° in the presence of HU. The bend angle calculated for the T_4A_4 tract duplex was 62 ± 4° after binding two HU dimers. Fluorescence anisotropy measurements reveal that HU binds in a 1:1 stoichiometry to the A_4T_4 tract duplex but a 2:1 stoichiometry to the T_4A_4 tract and random sequence duplex. These findings suggest that HU binding and recognition of DNA may be governed by a structural mechanism.

HU, a multi-functional DNA-binding protein, participates in several cellular functions including growth, recombination, replication, and transposition (*1*). Originally identified as a histone-like protein (*2*), more recent studies implicate HU as a DNA chaperone (*3*) or architectural protein, in which HU binding facilitates the formation of multiprotein complexes mediated by DNA looping or bending (*4*−*6*). Although HU participates in specific functions within the cell, as in the case of Gal repression and Mu transposition, HU does not exhibit sequence specific recognition of DNA. Functionally, HU parallels the behavior of the HMG protein found in eukaryotes, although there is no structural homology between the two proteins (*7*, *8*).

Recent binding experiments performed with cruciform, nicked or gapped DNA, and other repair intermediates indicate that HU may utilize a structure-based mechanism of recognition (*9*−*13*). In these studies, HU affinity for the DNA sequences was increased 50−100 fold relative to its affinity for linear duplex DNA, and a 1:1 binding stoichiometry was observed. Although HU exhibits an increased affinity for supercoiled (*14*) cruciform, nicked or gapped DNA (*9*−*12*, *15*), and DNA junctions (*13*), the binding affinity for sequences containing a static curve or bend is not clear. Earliest reports of HU binding to a 42 base pair sequence of curved DNA, as measured by gel mobility shift assay (GMSA), indicated that HU did not exhibit strong preferential binding to curved DNA (*16*). Subsequent reports of HU binding to bent DNA used longer oligo lengths (>100 bp) and observed a marked preference of HU for curved DNA. HU affinity was found to be at most 5-fold greater for curved DNA sequences relative to linear duplex DNA (*17*, *18*). In all cases, the static curve or bend was accomplished by the incorporation of A-tract sequences phased every 11 bp into the DNA.

Fluorescence resonance energy transfer (FRET)[1] has proven to be a very useful tool for measuring distances between 10 and 100 Å in DNA and monitoring conformational changes as a consequence of either sequence-induced or protein-induced bending (*19*−*23*). Specifically, sequence-induced curvature of DNA fragments containing phased A-tracts as a function of NaCl concentration was measured using FRET, and increased bending with increasing salt concentration was detected (*24*). In addition, DNA bending as induced by the binding of integration host factor (IHF), a protein that is identical in structure to HU, has been determined using the FRET methodology (*25*). From these measurements, an end-to-end distance was determined, which is in excellent agreement with that determined by X-ray

† This work was supported by a National Science Foundation Career Development Award, MCB-9507241 and a grant from the Patrick and Catherine Weldon Donaghue Medical Research Foundation. K.W. gratefully acknowledges support from an NIH training grant in Molecular Biophysics (GM08271).

* To whom correspondence should be addressed. Phone: (860) 685-2422. Fax: (860) 685-2141. E-mail: imukerji@wesleyan.edu.

‡ Present address: Optical Spectroscopy Section, NHLBI/NIH, Laboratory of Cell Biology, Building 10, Room 5D-14, Bethesda, MD 20892-1412.

[1] Abbreviations: bp, basepair; IHF, integration host factor; FRET, fluorescence resonance energy transfer.

10.1021/bi0264014 CCC: $25.00
Published on Web 02/19/2003

crystallography (*26*). Thus, these and other measurements demonstrate that FRET can be used reliably to determine the conformation of DNA alone and in protein−DNA complexes.

In our previous work, we examined the binding of HU to linear DNA duplexes using a fluorescent guanosine analogue (*27*). In those studies, the fluorescence intensity was observed to increase with HU binding, consistent with either DNA bending or unwinding. This result, coupled with the enhancement of DNA circularization by HU observed previously (*11*, *28*, *29*), was strongly suggestive of HU-induced bending of DNA. The current study addresses the magnitude of the protein-induced bend and the relative affinity of HU for bent DNA using fluorescence anisotropy and resonance energy transfer.

DNA curvature is accomplished by the presence of two phased A-tracts in a 20 bp duplex 5′-d($CA_4T_4GGA_4T_4C$)-3′, hereafter referred to as A4−20 (Table 1). Binding to this duplex is compared with a duplex of the same base composition, but the polarity of the A-tract is reversed 5′-d($CT_4A_4GGT_4A_4C$)-3′, referred to as T4−20 (Table 1). Previous reports have shown that T_4A_4 tracts do not exhibit anomalous gel migration behavior (*30*) or a premelting transition (*31*), and from these and other measurements (*32*), it was inferred that T_4A_4 tracts do not exhibit sequence-induced bending. HU binding affinity for the A_4−20 and T_4−20 duplexes, as measured by fluorescence anisotropy, is also compared with that for a random 20 bp sequence. The amount of bending induced upon HU binding is inferred from the end-to-end distance of the DNA measured by FRET in the presence or absence of HU. The end-to-end distance of the A4−20 duplex is shorter than that predicted from structural parameters of canonical B-form DNA and is shorter than the end-to-end distance of the T4−20 duplex, indicative of a sequence-induced bend of 45°. HU-induced bending is observed for both the A4−20 and the T4−20 duplexes, resulting in a final bend angle of 70 and 62°, respectively.

MATERIALS AND METHODS

HU Protein. HU protein was isolated from *Escherichia coli* strain, RLM1078, and purified according to the procedure previously described (*27*). From a liter culture of growth media, approximately 20 mg of HU was purified, and the purity was greater than 95% as determined by SDS−PAGE and amino acid analysis. Briefly, dialyzed cell lysate was loaded onto a SP-Sepharose (Amersham−Pharmacia) cation exchange column. HU containing fractions were pooled, dialyzed, and loaded onto a DNA−cellulose column, which was prepared by UV cross-linking calf thymus DNA to cellulose (Whatman CF-11) (*33*). To eliminate a contaminating nuclease that co-purifies with HU, a FPLC MonoS 5/5 cation exchange column (Amersham−Pharmacia) was used, and the nuclease-free HU eluted at approximately 0.35 M NaCl. The lack of nuclease activity was verified by the absence of any digested products after incubating the purified protein with plasmid DNA. HU protein concentration was determined by amino acid analysis (Keck Facility, Yale University). An extinction coefficient at 230 nm was determined to be 37.5 mM^{-1} cm^{-1} based on seven independent analyses.

Oligonucleotides. Oligonucleotides were purified by UV-shadowing and eluted from the gel by copious washes with 0.3 M sodium acetate, pH 6.5, at 37 °C or electroelution (Schleicher and Schuell, Concord, NH). Duplex formation was achieved by mixing equal molar amounts of pure single-stranded oligonucleotides, heating at 90 °C for 5 min, followed by slow cooling to room temperature in a water bath at a rate of approximately 0.2°/min. Concentrations of single-strand oligonucleotides were determined by measuring the absorbance at 260 nm at 90 °C. Extinction coefficients were calculated using the methodology of Richards (*34*).

Labeling of Oligonucleotides. Oligonucleotides used for FRET experiments were labeled with either 5- (and -6) carboxytetramethylrhodamine, succinimidyl ester (TMR) or 5- (and -6) carboxyfluorescein, succinimidyl ester (FAM) (Molecular Probes, Eugene, OR). Oligonucleotides synthesized with an amino modified C6 linker at the 5′-end were obtained from Integrated DNA Technologies (Coralville, IA). Table 1 lists the sequences of the duplexes and the positions of the dyes for the doubly labeled duplexes used in the FRET experiments. Singly labeled duplexes were prepared by annealing the labeled single strand with its unlabeled single-strand complement.

The labeling procedure was followed as described in the Molecular Probes technical bulletin (MP 00143) (*35*). To 1 mg of single-stranded oligonucleotide with the amino modified linker, a chloroform extraction was performed to remove excess ammonium salts followed by concentration by ethanol precipitation.

A 40:1 mole ratio of fluorescent probe to oligonucleotide was used per labeling reaction in the presence of 0.075 M sodium tetraborate, pH = 8.5, with a DNA concentration of 0.15 mM. The reaction was left constantly shaking overnight at room temperature. Labeled oligonucleotides were precipitated with ethanol to eliminate excess fluorescent label.

Labeled oligonucleotides were purified using a 20% denaturing polyacrylamide gel electrophoresis, followed by UV-shadowing and then electroelution as described above. The labeled oligonucleotides could also be viewed with visible light because of the fluorescent labels. Equal molar amounts of purified single-stranded oligonucleotides were annealed to their respective complements by heating to 90 °C for 5 min and allowed to anneal by slow cooling to room temperature. To ensure the absence of single strand in the sample, duplex DNA was purified on a 15% native polyacrylamide gel (19:1 acrylamide/Bis-acrylamide) at 4 °C. The main band was cut out of the gel and electroeluted overnight at 4 °C and 100 V, as described above.

To obtain an accurate concentration of labeled duplex DNA, the background contribution from fluorescein and rhodamine was subtracted from the overall absorbance at 260 nm. A correction factor for each dye was determined by using the absorbance ratios of 260:555 nm for rhodamine or 260:494 nm for fluorescein. The final duplex concentration was determined using the extinction coefficient of the duplex (ϵ_{ds}) based on the percent hypochromicity of the thermal melt from the unlabeled duplex

$$\text{hypochomicity} = \frac{A_{ss} - A_{ds}}{A_{ss}} \times 100 \qquad (1)$$

where A_{ss} and A_{ds} represent the absorbance of the single

strand and double strand, respectively. The labeling efficiency was determined by measuring the concentration of each dye relative to that of the duplex DNA. For the dyes, the molar extinction coefficients were taken from Molecular Probes (*35*)

Steady-State Fluorescence Anisotropy and Intensity Measurements. Steady-state fluorescence anisotropy and intensity measurements were performed with a FluoroMax-2 fluorometer (Instruments SA, Metuchen, NJ). Fluorescence was measured at a 90° angle in an L-format. Sample temperatures were maintained with a circulating bath at 10 °C (RTE Model 111, NESLAB Instruments, Inc.). After fluorescence experiments were performed, samples were routinely assayed using nondenaturing polyacrylamide gel electrophoresis, to confirm that protein−DNA complexes had not degraded from excess light exposure. All samples were in 10 mM Tris-HCl, pH 7.6 buffer containing 100 mM NaCl and 0.1 mM EDTA and were continuously stirred in a 3 × 3 mm Spectrosil S1 quartz cuvette (Starna Cell, Inc., CA).

Anisotropy data of the fluorescein duplexes were obtained using an excitation wavelength of 468 nm, and fluorescence was monitored from 516 to 522 nm. Anisotropy data of the rhodamine duplexes were obtained using an excitation wavelength of 560 nm, and fluorescence was monitored from 578 to 582 nm. The integration time for the anisotropy experiments was 10 s/pt, and data points were obtained in 2 nm increments; final values result from an average of six scans. Anisotropy data of the 6-MI labeled duplexes were obtained using an excitation wavelength of 330 nm, and fluorescence emission was monitored from 412 to 422 nm. The integration time was 10 s/pt, and data points were obtained in 3 nm increments; final values result from an average of six scans. The average standard deviation of anisotropy measurements was ±0.0025.

Intensity measurements were performed at magic angle with the excitation polarizer set to 0° and the emission polarizer set to 55°. Fluorescein emission spectra were obtained from 475 to 650 nm using an excitation wavelength of 468 nm. Rhodamine spectra were obtained from 570 to 650 nm using an excitation wavelength of 560 nm. The integration time for the intensity measurements was 1 s/pt, and samples were scanned at a rate of 1 nm/pt. The bandpass for both excitation and emission was 5 nm. Emission spectra of the 6-MI fluorescent duplexes were obtained from 350 to 550 nm using an excitation wavelength of 330 nm. The integration time for the intensity measurement was 1 s/pt, and samples were scanned at a rate of 2 nm/pt. The bandpass for both excitation and emission was 5 nm.

Analysis of binding parameters using fluorescence anisotropy for HU binding to the T4−20 and H1−20 duplexes was performed as previously described (*27*). HU binding to the A4−20 duplex was analyzed using the following equation:

$$f = \frac{([\mathrm{HU}]_T + [\mathrm{DNA}]_T + K_d) - \sqrt{([\mathrm{HU}]_T + [\mathrm{DNA}]_T + K_d)^2 - 4[\mathrm{DNA}]_T[\mathrm{HU}]_T}}{2[\mathrm{DNA}]_T} \quad (2)$$

In this case, $f = [\mathrm{HU{-}DNA}]/[\mathrm{DNA}]_T$. To analyze the spectroscopic data, it is assumed that the change in anisotropy is linearly proportional to the fraction of bound DNA. Thus, $f = (r - r_o)/[(r_\infty - r)R + (r - r_o)]$, where r is anisotropy, r_o is the anisotropy of the free DNA, r_∞ is the anisotropy of bound DNA at saturation, and $R = \phi_\infty/\phi_o$, where ϕ_o is the relative quantum yield of free DNA, and ϕ_∞ is the relative quantum yield of bound DNA at saturation (*36*).

FRET Analysis: Determination of R_o for A4−20 and T4−20. R_o (Förster distance) was calculated using the following equation (*37*):

$$R_o = 0.211(\kappa^2 \eta^{-4} \Phi_D J(\lambda))^{1/6} \quad (3)$$

where κ^2 is the relative orientation factor, typically 2/3 for dynamic random averaging of the donor and acceptor; η is the refractive index of the medium, assumed to be 1.4 for biomolecules in aqueous solution (*20*, *37*); and Φ_D is the quantum yield of the donor in the absence of acceptor. For both duplexes, Φ_D was measured using the donor only duplexes and found to be essentially that of fluorescein, 0.85 (*38*). The constant 0.211 is applied when the units of the wavelength are expressed in nanometers. $J(\lambda)$ is the degree of spectral overlap between the donor emission and acceptor absorption, expressed as $M^{-1}cm^{-1}(nm)^4$. The spectral overlap between the donor emission and the acceptor absorption spectra of the singly labeled duplexes were determined as follows (*37*):

$$J(\lambda) = \frac{\int_0^\infty F^D(\lambda)\epsilon^A(\lambda)\lambda^4 d\lambda}{\int_0^\infty F^D(\lambda) d\lambda} \quad (4)$$

where $F^D(\lambda)$ is the fraction of total donor fluorescence occurring at each wavelength, from λ to $(\lambda + \Delta\lambda)$, and $\epsilon^A(\lambda)$ is the extinction coefficient spectrum of the acceptor only duplex.

FRET Analysis: Determination of Efficiency of Transfer (E) and End-to-End Distance (R). The normalized enhanced acceptor fluorescence as a result of energy transfer was determined as a ratio of the enhanced acceptor emission relative to the acceptor only emission (*19*). This ratio was determined by using the emission of the extracted acceptor at 580 nm, from which the donor only spectral contribution was subtracted from 500 to 650 nm of the doubly labeled FRET molecule and dividing it by the emission at 580 nm when the doubly labeled molecule was excited at the acceptor excitation wavelength, 560 nm, depicted in eq 5.

$$(\mathrm{Ratio})_A = \frac{F_{em}(\nu_1, \nu')}{F_{em}(\nu_2, \nu'')} \quad (5)$$

Where the wavelengths ν_1 and ν_2 are 580 nm, ν' is the donor excitation wavelength (468 nm), and ν'' is the acceptor excitation wavelength (560 nm).

The efficiency of energy transfer, E, is related to $(\mathrm{Ratio})_A$ by the following equation (*19*, *39*):

$$(\mathrm{Ratio})_A = \left[\mathrm{E}d^+ \frac{\epsilon^D(\nu')}{\epsilon^A(\nu)} + \frac{\epsilon^A(\nu')}{\epsilon^A(\nu)}\right]\frac{\Phi^A(\nu_1)}{\Phi^A(\nu_2)} \quad (6)$$

Where ϵ^D and ϵ^A are the extinction coefficients of the donor and acceptor at their respective excitation wavelengths described above, and d^+ is the fraction of donor labeled molecules. Since the two emission wavelengths ν_1 and ν_2

Table 1: Sequences Used in FRET and Binding Affinity Experiments

oligonucleotide	sequence
A_4−20	FAM-5′- c aaa att ttg gaa aat ttt c -3′ [a] 3′- g ttt taa aac ctt tta aaa g -5′-TMR [b]
T_4−20	FAM-5′- c ttt taa aag gtt tta aaa c -3′ 3′- g aaa att ttc caa aat ttt g -5′-TMR
H1−20	5′- g aat caa cta ctt a**F**a tgg t -3′ [c] 3′- c tta gtt gat gaa tct acc a -5′

[a] FAM = carboxyfluorescein. [b] TMR = carboxytetramethylrhodamine. [c] **F** = 6-methyl-8-(2-deoxy-β-D-ribofuranosyl)-isoxanthopterin (6-MI) (*45*).

are equal, the quantum yield of the acceptor cancels in the above equation. From the calculated *E*, the donor to acceptor distance was determined using the following equation:

$$E = \frac{1}{[1 + (R/R_o)^6]} \quad (7)$$

RESULTS

HU Binding to Bent and Straight DNA Duplexes. HU binding stoichiometry and affinity to three 20 bp duplexes was characterized by fluorescence anisotropy where two of the duplexes have either A_4T_4 (A4−20) or T_4A_4 (T4−20) tracts, and one duplex, H1−20, is essentially random sequence (Table 1). Fluorescence anisotropy was measured with either rhodamine or fluorescein for the A4−20 and T4−20 duplexes and with 6-MI for the H1−20 duplex. The H1−20 duplex has no sequence similarities with the T4−20 and A4−20 duplexes, and the binding represents that of HU to general sequence B-DNA.

The stoichiometry of HU binding to each of the three duplexes was measured by titrating HU into a solution of either the A4−20, T4−20, or H1−20 duplexes at a concentration 10-fold greater than the K_d. At these relatively high concentrations of binding sites, the DNA binds all of the added HU protein. Thus, anisotropy as a function of HU molar ratio is discontinuous, in which it increases initially and then plateaus. The intersection of the linear region with the plateau is indicative of binding stoichiometry (Figure 1) (*27*, *40*, *41*). For the A4−20 duplex, this point indicates a 1:1 binding stoichiometry (Figure 1A); whereas for the T4−20 duplex, the data clearly indicate a 2:1 stoichiometry of HU/DNA (Figure 1A). Although the data shown is generated with the acceptor only duplexes, comparable results were obtained with the donor only duplexes (data not shown).

The stoichiometry plot of the H1−20 duplex is also indicative of at least 2 HU dimers binding. Since the anisotropy of the protein bound duplex is relatively high (0.27), we cannot exclude the possibility that higher order complexes may be present at higher protein concentrations. However, the most likely binding stoichiometry for the H1−20 duplex is 2:1 since two HU dimers bind to the T4−20 duplex, and previously, a 2:1 stoichiometry was detected for binding to a 13 bp duplex (*27*).

The equilibrium binding constants were measured using fluorescence anisotropy. For these experiments, the DNA concentration was held constant at or below the K_d of 0.1 μM. For the two A4−20 and T4−20 duplexes, protein binding initially leads to an increase in fluorescence anisotropy

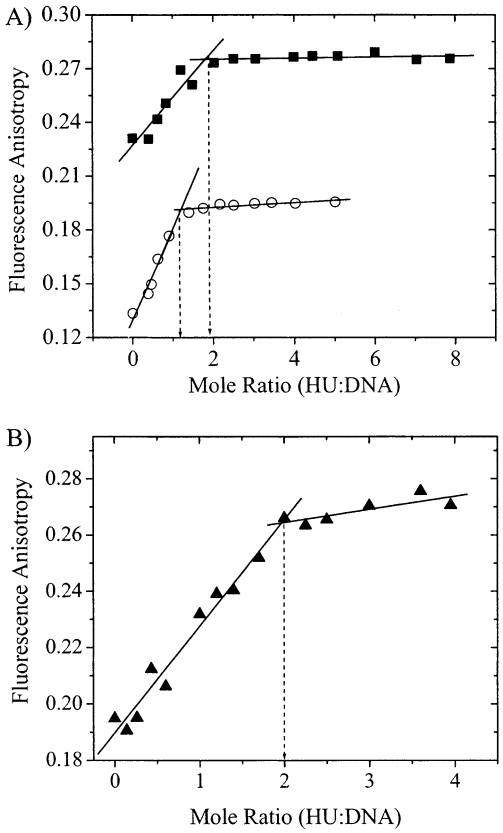

FIGURE 1: Determination of HU binding stoichiometry using fluorescence anisotropy. (A) A4−20 (○) and T4−20 (■) labeled with rhodamine. For clarity, in the graph A4−20 *r* values = *r* − 0.1. (B) H1−20 (▲) labeled with 6-MI. The intersection from the crossover of the slope and the plateau indicates the saturated molar ratio of HU to DNA for that duplex. The concentrations of DNA used in the stoichiometry experiments were at least 10-fold greater than the experimentally determined binding constants. All experiments were performed in a 10 mM Tris-HCl, 0.1 mM EDTA, pH 7.6 buffer containing 100 mM NaCl, at 10 °C.

that plateaus at a concentration of approximately 0.75 μM HU (Figure 2A). The relative increase in anisotropy (Δr = 0.16) is comparable for the two duplexes. For the H1−20 duplex, HU binding leads to an increase in fluorescence anisotropy, which plateaus at a concentration of approximately 2 μM (Figure 2B).

These saturable binding curves were used to determine the microscopic association constants for the interaction between HU and these duplexes (Table 2) (*40*−*43*). The experimentally determined stoichiometry values were used in determining equilibrium association constants. For both T4−20 and H1−20, binding to HU is well-described by a model of identical noninteracting binding sites (Figure 2A,B). These analyses reveal that HU exhibits increased affinity for the T4−20 duplex with a microscopic association constant of 4.4 ± 1.6 μM^{-1} that is almost 7-fold higher than that determined for the H1−20 duplex, 0.68 ± 0.29 μM^{-1} (Table 2). Only one HU dimer binds to the A4−20 duplex, and the data are fit using a 1:1 binding model. Interestingly, the association constants obtained for the binding of the first HU dimer to either the A4−20 or the T4−20 duplexes are within error of each other (6.1 ± 1.4 μM^{-1} vs 8.8 ± 1.6 μM^{-1}). Given HU's role as an architectural protein and proposed affinity for bent or distorted DNA structures, this finding is unexpected but may be a consequence of com-

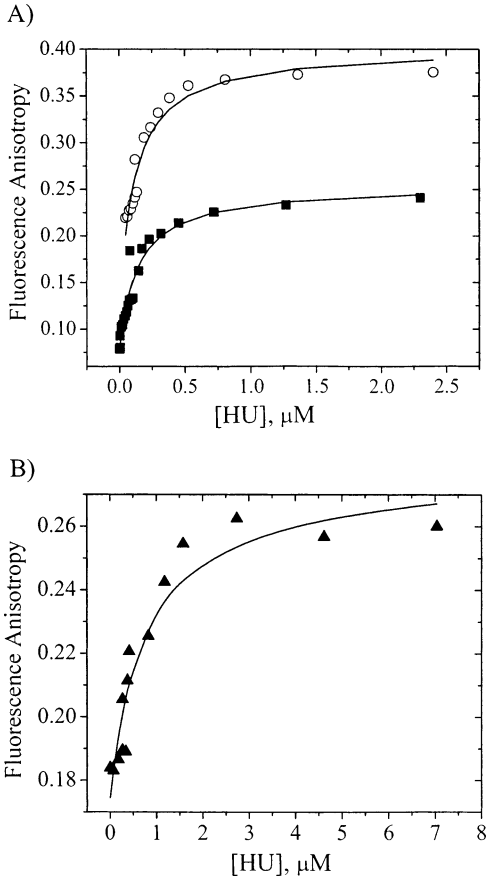

FIGURE 2: Equilibrium binding of HU to DNA monitored by fluorescence anisotropy. (A) A4−20 (○) labeled with FAM, [DNA] = 0.1 μM and T4−20 (■) labeled with FAM, [DNA] = 0.1 μM. For clarity in the graph, A4−20 r values shown = r + 0.13 (B) H1−20 (▲) labeled with 6-MI, [DNA] = 0.4 μM. Data are shown fit with binding isotherms as described in the text. Equilibrium binding constants are given in Table 2. Buffer conditions are the same as those described in Figure 1.

Table 2: HU Equilibrium Binding Constants Determined for A4−20, T4−20, and H1−20

duplex	anisotropy (μM^{-1})	FRET (μM^{-1})	GMSA (μM^{-1})[a]
A4−20	6.1 ± 1.4	4.0 ± 0.8[b]	3.3 ± 0.2[c]
T4−20	4.4 ± 1.6[d]	2.2 ± 1.2[b,d]	2.0 ± 0.1[c]
	$K1 = 2k = 8.8$[e]		
	$K2 = k/2 = 2.2$[e]		
duplex	anisotropy (μM^{-1})	intensity (μM^{-1})	GMSA (μM^{-1})[a]
H1−20	0.68 ± 0.29[d]	0.35 ± 0.06[d,f]	2.0 ± 0.4[c]
	$K1 = 2k = 1.36$[e]		
	$K2 = k/2 = 0.34$[e]		

[a] Gel mobility shift assay, data not shown. [b] Determined from the energy transfer efficiency as a function of HU concentration. [c] K_{app}, apparent binding constant. [d] Microscopic association constant. [e] Stepwise binding constant. [f] Determined from the change in fluorescence intensity at 442 nm as a function of HU concentration.

pensating enthalpy and entropy in the binding interaction (vide infra).

We observe that the binding constant obtained for H1−20 agrees well with our previous study of HU binding to linear DNA in which binding constants and stoichiometry were determined by fluorescence anisotropy and analytical ultracentrifugation (*27*). The association constant obtained for HU binding to the H1−20 duplex is comparable to those obtained for HU binding to 34 and 13 bp duplexes, indicating that HU binding affinity is independent of DNA length. The 6-MI nucleotide analogue used in the current study is structurally analogous to the 3-MI fluorescent probe used in the previous study; therefore, similar to 3-MI, it is not expected to affect HU binding (*27*, *44*, *45*).

A 40% increase in fluorescence intensity of the 6-MI probe is observed upon HU binding, indicative of a decrease in base stacking interactions or DNA unwinding (data not shown). The association constant determined from the fluorescence intensity change is comparable to that determined from the fluorescence anisotropy measurement (Table 2). The intensity increase results from reduced base stacking interactions and solvent exposure of the probe, which is probably a consequence of an HU-induced bend in the DNA. This result is similar to the fluorescence intensity increases observed for the 34 bp duplexes containing 3-MI studied previously (*27*).

Fluorescence Resonance Energy Transfer of A4−20 and T4−20. The degree of sequence-induced bending of the A4−20 and T4−20 duplexes was determined by measuring the end-to-end distance using FRET. Both duplexes were labeled with a fluorescein (FAM) derivative (donor) at the 5′-end of one strand and with a rhodamine (TMR) derivative (acceptor) at the 5′-end of the complementary strand (Table 1). The Förster distance (R_o), the distance at which energy transfer is 50% efficient or 50% of the donor molecules decay by energy transfer, is characteristic for a particular donor−acceptor pair. For A4−20, R_o was determined to be 52.5 Å, and for T4−20, R_o was found to be 51.6 Å; both R_o values were determined from the experimental data. Both the primary and the secondary structure of oligonucleotides as well as the length of the linker and the solution conditions can have an effect on the fluorescent properties of the conjugated dyes (*39*, *46*). In this case, the observed differences in R_o are attributed to the relative polarity of the A-tracts, which influence the conformation of the duplexes. The sequence-induced bending of the A-tract leads to a +2 nm shift in the emission maximum of the A4−20 duplex relative to the T4−20 duplex. This red-shift, coupled with a 10% increase in the acceptor extinction coefficient spectrum of the A4−20 duplex, accounts for the difference in the R_o values. Binding experiments performed with the donor-only and acceptor-only duplexes demonstrated that protein binding leads to an increase in R_o values of 0.5 Å. This increase in R_o is probably a result of the fluorescein emission maximum shifting to the red, as a consequence of protein binding and induced bending (Figure 3).

In these measurements, the labeled duplexes were excited at 468 nm rather than the absorbance maximum of fluorescein at 490 nm to avoid excitation of rhodamine and minimize its background fluorescence. Figure 3 depicts the emission spectra of the T4−20 donor-only duplex, doubly labeled duplex in the absence of HU, and doubly labeled duplex with HU completely bound. In comparing the spectra of the doubly labeled species, there is a significant increase (37%) in the 580 nm emission of rhodamine when HU is bound and the fluorescein emission maximum shifts +3 nm. The intensity increase at 580 nm is indicative of energy transfer and consequently, increased proximity of the two fluorescent probes.

Efficiency of Energy Transfer and End-to-End Distance. Protein titrations were performed with the doubly labeled

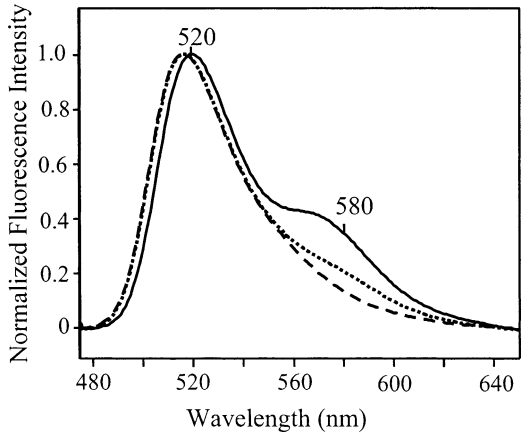

FIGURE 3: Fluorescence spectrum of the T_4−20 duplex obtained with 468 nm excitation. Doubly labeled duplex (dotted line), doubly labeled duplex with HU bound (solid line), and donor-only duplex (dashed line) are shown. The increased fluorescence emission observed at 580 nm is a consequence of energy transfer.

duplexes to determine the efficiency of energy transfer as a function of protein concentration. The efficiency values (*E*) were calculated by first determining $(\text{Ratio})_A$, the normalized fluorescence from the acceptor as a result of energy transfer (eq 6). This ratio was determined by dividing the extracted acceptor emission at 580 nm by the acceptor only emission at 580 nm of the doubly labeled duplex. The extracted acceptor emission spectra were generated by subtracting the donor only contribution as described in the Materials and Methods (*19*).

The binding affinity of HU for the A4−20 and the T4−20 duplexes was also determined from the efficiency of energy transfer (Figure 4). For both duplexes, the transfer efficiency reaches a maximum at saturating concentrations corresponding to an HU/DNA mole ratio greater than 2.5. A 1:1 binding model was used to analyze the A4−20 data, and for the T4−20 duplex, the curves were fit with a model of identical, noninteracting binding sites to obtain equilibrium association constants. The binding constants determined from the transfer efficiencies are within error of those determined by fluorescence anisotropy (Table 2), and the similarity of the values is consistent with a protein-induced conformational change that leads to a shorter distance between the probes and increased transfer efficiency.

In the absence of bound HU, the A4−20 duplex has a higher *E* value than the T4−20 duplex (0.10 vs 0.06). The calculated efficiencies (*E*) were used to determine the end-to-end distance (*R*) (eq 7). In the absence of protein, the higher *E* value obtained for the A4−20 duplex indicates that the donor and acceptor probes are closer in proximity in A4−20 relative to the T4−20 duplex. The increased energy transfer efficiency, and consequently, shorter end-to-end distance of the A4−20 duplex is consistent with the presence of a static bend.

Upon protein binding, the transfer efficiencies increase to a maximum value of 0.20 for the A4−20 duplex and 0.14 for the T4−20 duplex (Figure 4). With saturating amounts of HU protein, the end-to-end distance of the T4−20 duplex approaches that of the A4−20 duplex (69.8 Å vs 66.9 Å), indicating that the protein-induced conformation is comparable for both duplexes (Table 3).

The distance determination rests in part on the relative orientation of the dyes, which is represented in the κ^2 value

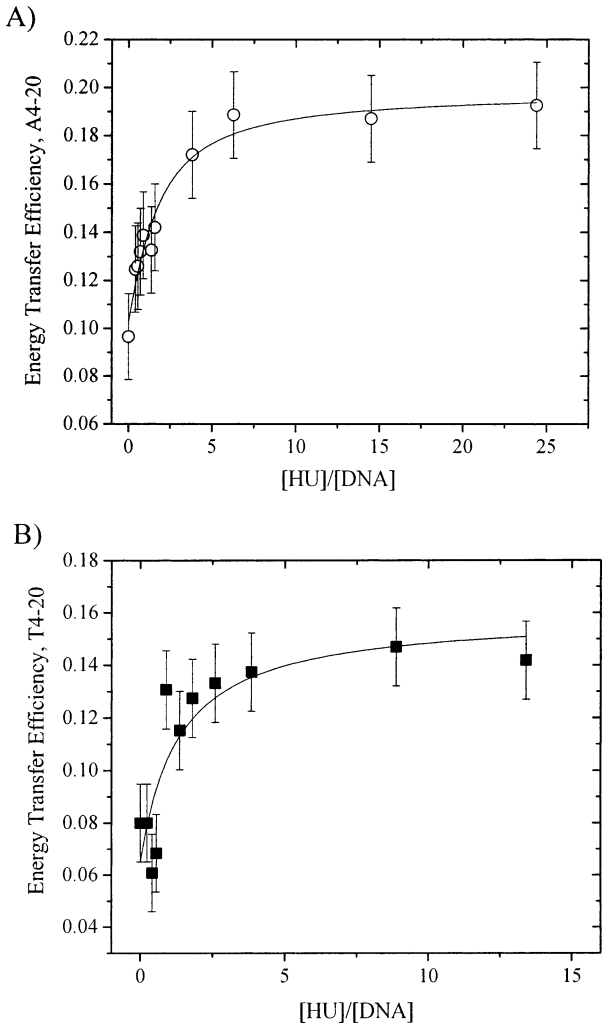

FIGURE 4: Energy transfer efficiencies (*E*) as a function of HU/DNA mole ratio. (A) A4−20 (○) and (B) T4−20 (■). Transfer efficiencies were calculated as described in the text. Buffer conditions are the same as those described in Figure 1. Data are shown fit with binding isotherms as a visual aid; equilibrium binding constants given in Table 2 were determined as a function of HU concentration.

(eq 3). If the dyes are freely rotating, then all possible dipole orientations can occur equally. For this study, the relative position of the dyes is inferred from previous modeling and experimental studies coupled with the fluorescence anisotropy measurements. FRET measurements coupled with molecular modeling indicate that the fluorescein linker adopts an extended conformation, such that fluorescein is freely rotating and located approximately 10 Å away from the 5′ terminus (*21*, *47*). In this study, FAM-labeled duplexes had a relatively low anisotropy value (0.07), which is indicative of free rotation (Figure 2A). The anisotropy of TMR-labeled duplexes was significantly higher, consistent with a stronger interaction between the dye and the DNA (Figure 1A). In previous work, it was observed that it is energetically favorable for rhodamine attached to DNA with a C6 linker to stack on top of the DNA helix (*21*, *25*, *48*). However, the rhodamine probably experiences enough wobble motion such that the orientation of the transition dipoles of the donor and acceptor are randomized with respect to the time of transfer (*19*, *22*). Thus, a κ^2 value of 2/3, consistent with rapid randomization of the relative orientation of the donor and acceptor (*19*−*21*), was used to calculate distances. The end-

Table 3: Dependence of R_C and Curvature Angle on C-6 Linker Length

	Without HU		With HU	
	A4−20 R^a = 75.3 Å	T4−20 R = 80.9 Å	A4−20 R = 66.9 Å	T4−20 R = 69.8 Å
		R_C = 78.1 Å[b]		
R/R_C	0.965	1.03	0.856	0.894
α[c]	30 ± 12°	nd[d]	62 ± 3°	53 ± 5°
		R_C = 81.5 Å[e]		
R/R_C	0.925	0.992	0.821	0.857
α[c]	45 ± 7°	14 ± 17°	70 ± 3°	62 ± 4°
		R_C = 84.9 Å[f]		
R/R_C	0.888	0.953	0.788	0.823
α[c]	55 ± 6°	35 ± 21°	76 ± 3°	69 ± 4°

[a] Distances reported are based on three independent measurements. [b] $R_C = L_0$ + linker; L_0 = length of the DNA (19 bp × 3.4 Å), where linker = 13.5 Å (*24*). [c] Bend angle determined using the following relationship, $R/R_C = \cos(\alpha/2)$. [d] Angle not determined because $R > R_C$. [e] $R_C = L_0 + 1.25 \times$ linker. [f] $R_C = L_0 + 1.5 \times$ linker.

to-end distance of the T4−20 duplex as measured by FRET using a κ^2 value of 2/3 is 80.9 ± 2.7 Å, which is in excellent agreement with the calculated DNA contour length of 81.5 Å (Table 3).

DISCUSSION

Relative Curvature of A4−20 and T4−20. Determination of the bend angle from the end-to-end distance is model dependent. In this study, the curvature angle (α) is determined from the ratio of the end-to-end distance (R) to the contour length (R_C) using the following expression, in which it is assumed that the bend occurs in the middle of the DNA (*49*, *50*):

$$\frac{R}{R_C} = \cos\left(\frac{\alpha}{2}\right)$$

The contour length is that of the DNA helix with the lengths contributed by the fluorescent probes and their associated linkers added. Thus, the extent of bending, explicitly dependent on the contour length, R_C, is determined in part by the position of the dyes with respect to the DNA helix. Previous molecular dynamics modeling studies of the dye molecules and their C-6 amino linkers have indicated that generally fluorescein points away from the DNA, while rhodamine tends to stack on top of the DNA helix (*21*, *25*, *48*).

In Table 3, R/R_C ratios and corresponding bend angles are calculated assuming a completely extended fluorescein linker and different lengths of the rhodamine linker. These ratios demonstrate the dependence of curvature angle on DNA contour length. If half of the rhodamine linker is included in the total length, then the calculated R_C is 84.9 Å, and the bend angle for the T4−20 duplex is 35°. Conversely, if the rhodamine is assumed to stack on the end of the DNA helix with no associated linker length, then the R_C is smaller than the experimentally determined end-to-end distance (R), and no angle can be calculated. Parkhurst and others have noted this dependence of bend angle on contour length previously, where relatively small changes in length leads to large changes in bend angle (*49*, *51*).

If R_C is taken as 81.5 Å, where one-fourth of the rhodamine C-6 linker contributes to the total length, then the T4−20 duplex bend angle is 14 ± 17°, which is consistent with the bend angle of 19.7° as determined from molecular dynamic calculations of the same sequence without the fluorescent probes and associated linkers (D. Kombo, personal communication). Since a contour length of 81.5 Å is also consistent with an extended position for fluorescein and a stacked position for rhodamine (see above), this length was used for the comparison of bend angles.

For the A4−20 duplex, the end-to-end distance (R) is 75.3 Å, giving a R/R_C ratio of 0.925 and a curvature angle of 45 or 22.5° per helical turn. In comparison, the T4−20 duplex has an end-to-end distance of 80.9 Å, giving an R/R_C value of 0.992, indicative of a relatively linear duplex. Although the absolute bend angle is not known with certainty because of the contour length, relative measurements are accurate and indicate that A4−20 is more curved than T4−20 by at least 30°.

The current findings are consistent with earlier reports that T_nA_n tracts are relatively straight, while A_nT_n tracts are curved (*30*−*32*). In earlier studies of A_4T_4 and T_4A_4 tracts (*30*, *31*, *52*), a YR or RY step of CG or GC separated the tracts. In the current study, the A-tracts remain phased with the helix; however, a GG base step exists between the two tracts (Table 1), and similar to other previously studied bent A-tract sequences a YR step occurs at the end of the A_4T_4 tract. The current results demonstrate that the presence of a YR or RY step between A_4T_4 tracts is not required for DNA bending.

The measured bend angle of 22.5° per A-tract is in good agreement with cyclization and transient electric dichroism experiments, which measured a bend per A-tract of 28 and 18°, respectively, but is not consistent with electrophoretic studies in which an 11° bend per A-tract was observed (*53*−*55*). In the FRET determination, the absolute curvature angle largely depends on the model used and the estimation of contour length, which depends on the relative position of the dyes as discussed above. Nevertheless, the current findings are consistent with other solution-based studies that indicate the presence of one A-tract leads to a bend of 20−30°.

Protein-Induced Bending. HU induces a bend in both the A4−20 and the T4−20 duplexes upon binding, and the resultant bend angles are within 8° of each other. One HU dimer binds to the A4−20 duplex, and the end-to-end distance is reduced by 8 Å, which corresponds to an induced bend of 25°. In contrast, two HU dimers bind to the T4−20 duplex and induce a bend of ∼50° as calculated from the end-to-end distance of 69.8 Å. Interestingly, the binding of one HU dimer leads to an induced bend of 25° for both duplexes, and the total bend angle achieved upon protein saturation is comparable. Thus, it appears that HU binding stoichiometry is determined not by DNA length but by the number of dimers needed to achieve the desired bend angle. Therefore, in the case of the pre-bent A4−20 duplex, only one HU dimer is required to achieve a total bend of 70°, while for the linear 20 bp duplexes (T4−20 and H1−20) at least two HU dimers are needed.

This HU-induced bend angle is consistent with the bend angle of 65° as determined previously by Rouvière-Yaniv and co-workers using a circular permuation assay (*11*). Footprinting experiments of HU bound specifically to nicked and cruciform DNA determined that the binding motif

recognized by HU is a pair of inclined DNA helices (*11*). In the current study, the angle formed by the A-tract duplex may be comparable to that of two arms of a junction leading to the observation of a structurally specific HU/DNA interaction. We cannot rule out the possibility that the pre-bent structure of the A-tract prohibits the binding of additional HU dimers.

The HU-induced bend angle determined in this study is considerably smaller than that observed for integration host factor (IHF), which is structurally identical to HU. IHF binds to a specific DNA sequence and bends duplex DNA by at least 160°, as determined from the cocrystal structure and gel retardation assays (*26*, *50*). In a previous study, which transformed HU into a chemical nuclease, an average bend angle of 156° was measured in the context of the Mu transpososome, which consists of supercoiled DNA, transposase, IHF, and other proteins (*5*). This bend angle is comparable to that of the IHF-induced bend and is considerably larger than that observed in this study. It is possible that the presence of other protein components, such as in the Mu transpososome or the Gal repressosome leads to a greater degree of bending. In this study, one HU dimer induces a bend of 25°, which is 1/6 of the angle induced by IHF. Since HU binds to DNA independent of sequence, the differences in the binding and induced bend between IHF and HU may be a consequence of sequence specific interactions between IHF and its consensus DNA. In addition, the estimation of the bend angle does not take into account the possibility of kinking the DNA at discrete positions, as was observed in the IHF−DNA cocrystal structure (*26*).

Binding Stoichiometry and Structural Selectivity. In previous studies, distortion of the DNA helix has led to a 100-fold increase in HU binding affinity and well-defined binding stoichiometries (*9*−*14*). In this study, we observe that HU binding affinity for A4−20 is only modestly stronger (9-fold) than that observed for a random sequence duplex (6.1 vs 0.68 μM^{-1}), and the affinity for the A4−20 duplex is comparable to that for the T4−20 duplex (Table 2). The 1:1 binding stoichiometry observed for A4−20 is suggestive of some selectivity; however, the comparable affinity exhibited for A4−20 and T4−20 is perplexing. We suggest that competing entropy and enthalpy terms in the binding reaction lead to the comparable affinities. In the case of the A4−20 duplex, an unfavorable enthalpic component may arise from the alignment of the HU β-arms in the relatively rigid and narrowed minor groove of the A-tract (*56*, *57*). Conversely, the binding of HU to the T4−20 duplex is favorable enthalpically, but the induced bend leads to a greater loss in conformational entropy relative to the A4−20 duplex.

Binding to either A4−20 or T4−20 is 7−9-fold tighter than binding to the random sequence H1−20 duplex. This finding is suggestive of a slightly higher affinity for AT-rich sequences, which is consistent with the function of HU as an architectural protein since adenine rich sequences are often found in promoter regions and at the origin of replication (*58*). Given the increased affinity of HU for A4−20 and the 1:1 binding stoichiometry, we suggest that HU does exhibit modest selectivity in binding to this sequence, and the selectivity is based on the DNA structure and not the sequence. This is in keeping with previous studies where HU binding to bent or more flexible DNA substrates has been defined as specific because of the increase in affinity and the well-defined binding stoichiometry (*9*, *14*). Since the increase in affinity is not as great as that observed previously, we suggest that HU binding specificity and affinity scales with the degree of bending and the flexibility of the DNA substrate. Thus, HU has a higher affinity for more strongly bent or flexible substrates relative to the A-tract DNA used in this study.

In summary, these FRET and fluorescence anisotropy measurements have shown that duplexes containing A_4T_4 tracts are curved by at least 30° relative to a duplex containing T_4A_4 tracts. HU binding to either the T4−20 or the A4−20 duplex leads to an induced bend, such that the total bend angle ranges from 60 to 70°. In the case of the A4−20 duplex, this corresponds to an induced bend of 25° and a 50° induced bend for the T4−20 duplex. Furthermore, HU binds to both of these sequences with a higher affinity relative to a random sequence duplex. HU forms a 1:1 complex with the bent duplex, A4−20, but a 2:1 complex with the linear duplexes, T4−20 and H1−20. This binding stoichiometry is suggestive of a structure-based mechanism of recognition that is consistent with the role of HU as an architectural protein.

ACKNOWLEDGMENT

We are grateful to Prof. Roger McMacken for the gift of the HU overexpressing *E. coli* strain RLM1078. We also thank Mary Hawkins for the gift of the 6MI-containing oligonucleotide.

REFERENCES

1. Drlica, K., and Rouviere-Yaniv, J. (1987) Histonelike Proteins of Bacteria, *Microbiol. Rev. 51*, 301−319.
2. Rouviere-Yaniv, J., and Gros, F. (1975) Characterization of a novel, low-molecular-weight DNA-binding protein from *Escherichia coli*, *Proc. Natl. Acad. Sci. U.S.A. 72*, 3428−3432.
3. Travers, A. (1993) in *DNA-Protein Interactions*, pp 28−51, Chapman & Hall, London.
4. Lavoie, B. D., and Chaconas, G. (1993) Site-specific HU binding in the Mu transpososome: conversion of a sequence-independent DNA-binding protein into a chemical nuclease, *Genes Dev. 7*, 2510−2519.
5. Lavoie, B. D., Shaw, G. S., Millner, A., and Chaconas, G. (1996) Anatomy of a Flexer-DNA Complex inside a Higher-Order Transposition Intermediate, *Cell 85*, 761−771.
6. Aki, T., and Adhya, S. (1997) Repressor induced site-specific binding of HU for transcriptional regulation, *EMBO J. 16*, 3666−3674.
7. Bianchi, M. E. (1994) Prokaryotic HU and eukaryotic HMG1: a kinked relationship, *Mol. Microbiol. 14*, 1−5.
8. Rice, P. A. (1997) Making DNA do a U-turn: IHF and related proteins, *Curr. Opin. Struct. Biol. 7*, 86−93.
9. Pontiggia, A., Negri, A., Beltrame, M., and Bianchi, M. E. (1993) Protein HU binds specifically to kinked DNA, *Mol. Microbiol. 7*, 343−350.
10. Castaing, B., Zelwer, C., Laval, J., and Boiteux, S. (1995) HU Protein of *Escherichia coli* Binds Specifically to DNA That Contains Single-strand Breaks or Gaps, *J. Biol. Chem. 270*, 10291−10296.
11. Kamashev, D., Balandina, A., and Rouvière-Yaniv, J. (1999) The binding motif recognized by HU on both nicked and cruciform DNA, *EMBO J. 18*, 5434−5444.
12. Pinson, V., Takahashi, M., and Rouviere-Yaniv, J. (1999) Differential Binding of the *Escherichia Coli* HU, Homodimeric Forms and Heterodimeric Form to Linear, Gapped and Cruciform DNA, *J. Mol. Biol. 287*, 485−497.
13. Kamashev, D., and Rouviere-Yaniv, J. (2000) The histone-like protein HU binds specifically to DNA recombination and repair intermediates, *EMBO J. 19*, 6527−6535.

14. Kobryn, K., Lavoie, B. D., and Chaconas, G. (1999) Supercoiling-dependent Site-specific Binding of HU to Naked Mu DNA, *J. Mol. Biol. 289*, 777−784.
15. Bonnefoy, E., Takahashi, M., and Rouviere-Yaniv, J. (1994) DNA-binding Parameters of the HU protein of *Escherichia coli* to Cruciform DNA, *J. Mol. Biol. 242*, 116−129.
16. Bonnefoy, E., and Rouviere-Yaniv, J. (1991) HU and IHF, two homologous histone-like proteins of *Escherichia coli*, form different protein-DNA complexes with short DNA fragments, *EMBO J. 10*, 687−696.
17. Tanaka, H., Goshima, N., Kohno, K., Kano, Y., and Imamoto, F. (1993) Properties of DNA-Binding of HU Heterotypic and Homotypic Dimers from *Escherichia coli*, *J. Biochem. 113*, 568−572.
18. Shimizu, M., Miyake, M., Kanke, F., Matsumoto, U., and Shindo, H. (1995) Characterization of the binding of HU and IHF, homologous histone-like proteins of *Escherichia coli*, to curved and uncurved DNA, *Biochim. Biophys. Acta 1264*, 330−336.
19. Clegg, R. M. (1992) Fluorescence Resonance Energy Transfer and Nucleic Acids, *Methods Enzymol. 211*, 353−388.
20. Selvin, P. R. (1995) Fluorescence Resonance Energy Transfer, *Methods Enzymol. 246*, 300−334.
21. Hillisch, A., Lorenz, M., and Diekmann, S. (2001) Recent advances in FRET: distance determination in protein-DNA complexes, *Curr. Opin. Struct. Biol. 11*, 201−207.
22. Parkhurst, L. J., Parkhurst, K. M., Powell, R., Wu, J., and Williams, S. (2002) Time-resolved Fluorescence Resonance Transfer Studies of DNA Bending in Double-Stranded Oligonucleotides and in DNA-Protein Complexes, *Biopolymers (Nucleic Acid Sciences) 61*, 180−200.
23. Klostermeier, D., and Millar, D. P. (2002) Time-Resolved Fluorescence Resonance Energy Transfer: A Versatile Tool for the Analysis of Nucleic Acids, *Biopolymers 61*, 159−179.
24. Toth, K., Sauermann, V., and Langowski, J. (1998) DNA Curvature in Solution Measured by Fluorescence Resonance Energy Transfer, *Biochemistry 37*, 8173−8179.
25. Lorenz, M., Hillisch, A., Goodman, S. D., and Diekmann, S. (1999) Global structure similarities of intact and nicked DNA complexed with IHF measured in solution by fluorescence resonance energy transfer, *Nucl. Acids Res. 27*, 4619−4625.
26. Rice, P. A., Yang, S.-W., Mizuuchi, K., and Nash, H. A. (1996) Crystal Structure of an IHF-DNA Complex: A Protein-Induced DNA U-Turn, *Cell 87*, 1295−1306.
27. Wojtuszewski, K., Hawkins, M. E., Cole, J. L., and Mukerji, I. (2001) HU Binding to DNA: Evidence for Multiple Complexes and DNA Bending, *Biochemistry 40*, 2588−2598.
28. Hodges-Garcia, Y., Hagerman, P. J., and Pettijohn, D. E. (1989) DNA Ring Closure Mediated by Protein HU, *J. Biol. Chem. 264*, 14621−14623.
29. Paull, T., Haykinson, M., and Johnson, R. (1993) The nonspecific DNA-binding and bending proteins HMG1 and HMG2 promote the assembly of complex nucleoprotein structure, *Genes Dev. 7*, 1521−1534.
30. Hagerman, P. J. (1986) Sequence-directed curvature of DNA, *Nature 321*, 449.
31. Park, Y.-W., and Breslauer, K. J. (1991) A Spectroscopic and Calorimetric Study of the Melting Behaviors of a 'bent' and 'normal' DNA Duplex: [d(GA4T4C)]2 versus [d(GT4A4C)]2, *Proc. Natl. Acad. Sci. U.S.A. 88*, 1551−1555.
32. Haran, T. E., and Crothers, D. M. (1989) Cooperativity in A-Tract Structure and Bending Properties of Composite T_nA_n Blocks, *Biochemistry 28*, 2763−2767.
33. Alberts, B., and Herrick, G. (1971) DNA-Cellulose Chromatography, *Methods Enzymol. 21*, 198−217.
34. Richards, E. G. (1975) in *Handbook of Biochemistry and Molecular Biology* (Fasman, G. D., Ed.) p 589, CRC Press, Cleveland, OH.
35. Haugland, R. P. (1996) *Handbook of Fluorescent Probes and Research Chemicals*, 7th ed., Molecular Probes, Inc., Eugene, OR.
36. Lakowicz, J. R. (1983) *Principles of Fluorescence Spectroscopy*, Plenum Press, New York.
37. Lakowicz, J. R. (1999) *Principles of Fluorescence Spectroscopy*, 2nd ed., Kluwer Academic/Plenum, New York.
38. Parker, C. A., and Rees, W. T. (1960) Correction of Fluorescence Spectra and Measurement of Fluorescence Quantum Efficiency, *Analyst 85*, 587−600.
39. Clegg, R. M., Murchie, A. I., and Lilley, D. M. (1994) The solution structure of the four-way DNA junction at low-salt conditions: a fluorescence resonance energy transfer analysis, *Biophys J. 66*, 99−109.
40. Jameson, D. M., and Sawyer, W. H. (1995) Fluorescence Anisotropy Applied to Biomolecular Interactions, *Methods Enzymol. 246*, 283−300.
41. Heyduk, T., and Lee, J. C. (1990) Application of fluorescence energy transfer and polarization to monitor *Escherichia coli* cAMP receptor protein and *lac* promoter interaction, *Proc. Natl. Acad. Sci. U.S.A. 87*, 1744−1748.
42. Heyduk, T., Ma, Y., Tang, H., and Ebright, R. H. (1996) Fluorescence Anisotropy: Rapid, Quanititative Assay for Protein-DNA and Protein-Protein Interaction, *Methods Enzymol. 274*, 492−503.
43. Eftink, M. R. (1997) Fluorescence Methods for Studying Equilibrium Macromolecule-Ligand Interactions, *Methods Enzymol. 278*, 221−258.
44. Hawkins, M. E., Pfleiderer, W., Mazumder, A., Pommier, Y. G., and Balis, F. M. (1995) Incorporation of a fluorescent guanosine analogue into oligonucleotides and its application to a real time assay for the HIV-1 integrase 3′-processing reaction, *Nucl. Acids Res. 23*, 2872−2880.
45. Hawkins, M. E., Pfleiderer, W., Balis, F. M., Porter, D., and Knutson, J. R. (1997) Fluorescence Properties of Pteridine Nucleoside Analogues as Monomers and Incorporated into Oligonucleotides, *Anal. Biochem. 244*, 86−95.
46. Nazarenko, I., Pires, R., Lowe, B., Obaidy, M., and Rashtchian, A. (2002) Effect of primary and secondary structure of oligodeoxyribonucleotides on the fluorescent properties of conjugated dyes, *Nucl. Acids Res. 30*, 2089−2195.
47. Norman, D. G., Grainger, R. J., Uhrin, D., and Lilley, D. M. J. (2000) Location of Cyanine-3 on Double-Stranded DNA: Importance for Fluorescence Resonance Energy Transfer Studies, *Biochemistry 39*, 6317−6324.
48. Stuhmeier, F., Hillisch, A., Clegg, R. M., and Diekmann, S. (2000) Fluorescence Energy Transfer Analysis of DNA Structures Containing Several Bulges and their Interaction with CAP, *J. Mol. Biol. 302*, 1081−1100.
49. Hardwidge, P. R., Wu, J., Williams, S. L., Parkhurst, K. M., Parkhurst, L. J., and Maher, L. J. (2002) DNA Bending by bZIP Charge Variants: A Unified Study Using Electrophoretic Phasing and Fluorescence Resonance Energy Transfer, *Biochemistry 41*, 7732−7742.
50. Thompson, J. F., and Landy, A. (1988) Empirical estimation of protein-induced DNA bending angles: applications to λ site-specific recombination complexes, *Nucl. Acids Res. 16*, 9687−9705.
51. Wu, J., Parkhurst, K. M., Powell, R. M., and Parkhurst, L. J. (2001) DNA Sequence-dependent differences in TATA-binding protein-induced DNA bending in solution are highly sensitive to osmolytes, *J. Biol. Chem. 276*, 14623−14627.
52. Burkhoff, A. M., and Tullius, T. D. (1988) Structural Details of an Adenine Tract That Does Not Cause DNA to Bend, *Nature 331*, 455−457.
53. Calladine, C. R., and Drew, H. R. (1986) Principles of sequence-dependent flexure of DNA, *J. Mol. Biol. 192*, 907−918.
54. Ulanovsky, L., Bodner, M., Trifonov, E. N., and Choder, M. (1986) Curved DNA: Design, synthesis, and circularization, *Proc. Natl. Acad. Sci. 83*, 862−866.
55. Levene, S. D., Wu, H. M., and Crothers, D. M. (1986) Bending and flexibility of kinetoplast DNA, *Biochemistry 25*, 3988−3995.
56. Nelson, H. C. M., Finch, J. T., Luisi, B. F., and Klug, A. (1987) The Structure of an oligo (dA).oligo (dT) Tract and its Biological Implications, *Nature 330*, 221−226.
57. Crothers, D. M., and Shakked, Z. (1999) in *Oxford Handbook of Nucleic Acid Structure* (Neidle, S., Ed.) pp 455−470, Oxford University Press, Oxford.
58. Sinden, R. R. (1994) *DNA Structure and Function*, Academic Press, San Diego.

BI0264014